Acta Polytechnica **66**(2):173–184, 2026
https://doi.org/10.14311/AP.2026.66.0173

Published by the Czech Technical University in Prague

ANTI-VEHICLE BARRIER FOR URBAN ENVIRONMENT: DESIGN, SIMULATIONS, AND FULL-SCALE TESTING

Petr Konrád[a], Zbyněk Proske[b], Marek Semela[c], Jindřich Fornůsek[a], Michal Mára[a,*], Luboš Nouzovský[d], Radoslav Sovják[a]

[a] *Czech Technical University in Prague, Faculty of Civil Engineering, Experimental Centre, Thákurova 7, 166 29 Prague, Czech Republic*

[b] *VSB – Technical University of Ostrava, Faculty of Civil Engineering, Department of Urban Engineering, Ludvíka Podéště 17, 708 00 Ostrava, Czech Republic*

[c] *Brno University of Technology, Institute of Forensic Engineering, Department of Expertise in Mechanical Engineering, Analysis of Traffic Accidents and Vehicle Assessment, Purkyňova 118, 612 00 Brno, Czech Republic*

[d] *Czech Technical University in Prague, Faculty of Transportation Sciences, Department of Forensic Experts in Transportation, Horská 3, 128 00 Prague, Czech Republic*

[*] corresponding author: maramich@cvut.cz

Abstract. The increasing need for security measures in urban environments has highlighted the importance of effective anti-vehicle barriers. This paper presents the design, numerical simulations, and testing of an anti-vehicle barrier tailored for rapid deployment in cities. The proposed design strikes a balance between the need for high security and transportation and urban space constraints, while minimizing visual impact, and allowing pedestrian access. The effectiveness of the barrier against vehicular threats is evaluated through numerical simulations and real crash tests. The results offer practical insights for designing such protective barriers.

Keywords: Anti-vehicle barrier, urban security, barrier design, vehicular threats, numerical simulations, urban environment, safety, security infrastructure.

1. Introduction

In recent years, the threat of targeted terrorist attacks using vehicles as weapons (VAW) has increased significantly. In response, the widespread installation of various Vehicle Security Barriers (VSBs) in urban environments has proven crucial in mitigating these risks [1]. The development of VSBs has focused on two main types of barriers: safety traffic barriers such as safety railings, which are used primarily to mitigate the effects of accidents and protect vehicle occupants [2, 3], and specialised crash barriers designed to stop vehicles in deliberate attacks, where traditional barriers are often insufficient [4]. Fixed bollards are commonly used for this purpose [5]. Fixed barriers can also be in the form of visually pleasing natural objects, such as boulders [6, 7]. However, fixed barriers cannot be used in all locations due to various city constraints. Mobile barriers offer flexibility and rapid deployment, making them ideal for protecting vulnerable areas [8] when necessary. Historically, the Czechoslovak "hedgehog" inspired the development of modern mobile barriers. This design, consisting of interconnected steel profiles, was effective against armoured vehicles [9]. A modern variant using High-Performance Fibre-Reinforced Concrete (HPFRC) offers a combination of low weight and high energy absorption [10]. Tests have shown that an optimised barrier geometry can stop a 1 300 kg vehicle moving at a speed of 48 km h^{-1} [11]. In addition, HPFRC-based composite materials exhibit a low crack formation and fragmentation, increasing safety and durability [12–14]. However, barrier analyses and design should take into account not only technical aspects but also social and urban design factors to ensure optimal integration into the urban environment and minimise negative impacts on the quality of life of residents [15].

Traditional validation of these systems relies on full-scale physical testing according to internationally recognised standards such as PAS68/IWA14-1. Unfortunately, these tests are conducted under idealised conditions. Simplified underlay layers may not be representative of realistic installation conditions and do not adequately account for the complications associated with the placement in urban landscapes, where existing underground networks can present significant design constraints [16]. Furthermore, while existing barrier testing standards such as ISO 22343 emphasise the importance of ground conditions, some standards lack a detailed guidance on how to deal with them [17]. Other standards, such as ASTM F2656-07, provide exhaustive procedures for impact testing and barrier classification. These standards ensure that barriers meet the minimum impact resistance requirements. According to Yoo et al. [18], to achieve a P1 classification (penetration of less than one meter when struck by a vehicle at 80.5 km h^{-1}), the barrier must

effectively stop the vehicle and minimise vehicle penetration. With regard to the normative framework, it is important to highlight that existing standards and regulations for testing and certification of anti-vehicle barriers are constantly evolving to better reflect current threats and technological advances. Therefore, it is important that research and development in this area are in line with the latest standards and take into account the specific requirements and constraints of urban environments [8].

Given these constraints, advanced numerical simulation techniques are needed as a valuable tool for the development and evaluation of anti-vehicle barriers. These simulations allow the assessment of a variety of practical configurations, including different impact velocities, angles, and site conditions, which would be tedious and costly in the case of a large series of physical tests [16, 17]. A key aspect of simulations is modelling the interaction of the barrier with the surface, as this interaction significantly affects the ability of the barrier to absorb energy and stop a vehicle. And it is the level of detail in modelling the behaviour of the surface over which the barrier moves that has a crucial impact [11]. However, even computationally intensive simulations may not be sufficient, and therefore, validation of models through experimental data is still necessary [19]. In their study, Yoo et al. [18], when comparing simulations with real impact tests, found that hybrid FEM-SPH modelling better predicts the barrier behaviour, especially for large ground deformations. This method combines the advantages of the Finite Element Method (FEM) and the Smoothed Particle Method (SPH), allowing a more accurate modelling of the interaction between the barrier and the surrounding area. Another important factor is the design of the vehicle itself and its deformation and interaction with the barrier. Dynamic load analysis can be used to evaluate the effectiveness of VSBs [5]. In addition to the peak force values, it is important to consider the time history of the load and the dynamic load factor (DLF). The DLF allows us to estimate the equivalent static load that would induce the same stress in the barrier structure as the dynamic impact. Markovic et al. [1] found that the DLF strongly depends on the shape of the load function and the natural frequencies of the barrier.

2. Barrier development and testing

2.1. Geometry and principle

The first step in designing the barrier was to decide on its basic geometry and principle. A mobile barrier that is not connected to the surface was chosen, because it aligns with the objectives of the accompanying research project. It is also the only option for quick deployment in areas where a permanent (albeit more efficient) barrier cannot be placed. Mobile barriers can work with different principles, for example, interacting more with the impacting vehicle or the surface. However, the most commonly used types rely simply on the mass principle, similar to concrete Jersey walls. However, the Jersey wall and others have a major disadvantage, which is presenting an impassable obstacle for pedestrians, meaning it is not suitable for an urban environment and, moreover, its direct vehicle impact performance is not high.

To address these challenges, a hybrid concrete-steel barrier was developed, combining the principles of mass and vehicle interaction. The weight was reduced for easier deployment while allowing pedestrian passage. The barrier does not require any surface preparation, such as drilling or anchoring.

The design of the barrier is shown in Figure 1 and its basic characteristics are summarised in Table 1. The principle of mass simply comes from its weight of roughly 1.5 tonnes. The barrier must be placed with the column facing away from the threat, meaning that the vehicle's front wheels first weigh down the barriers' base before impacting the column, which is one part of the vehicle interaction principle. In a way, the barrier is designed as a bollard, which carries its own mobile base. Figure 2 shows the steel elements embedded in the concrete. In blue is the main steel brace (see Table 1), which forms the main reinforcement of the column. It also presents the second part of the vehicle interaction, as it is planned that in the event of a very strong crash, the steel brace will rip from the concrete and its horizontal part will rotate to brace against the vehicle's underside, being supported by the steel rod located at the joint between the horizontal and vertical beams. The brace also has four small steel teeth welded to its bottom, which can be seen in Figure 2 in front view. These teeth are expected to aid the barrier-surface interaction in the event of the brace ripping from concrete and rotating along the rod. The braces prepared before the barrier is poured can be seen in Figure 3. In addition, the hollow volumes were covered by thin sheet metal, and sheet metal was also added at the profile's joint for manufacturing reasons. The barrier must be kept at a reasonable weight for transportation, therefore, a complete solution will comprise of multiple barriers connected together. This requires connection locks, which can be seen on the sides of the barrier's base. There is a hole in each lock to push a steel rod through for securing the barriers together. The rod is highlighted in orange, and the concrete reinforcement bars in red.

2.2. Vehicle impact numerical simulations

The barrier model was created in the AutoCAD software and exported to the ANSYS Spaceclaim and Mechanical software in order to create meshes and other necessary geometric preparations. The rest of the work continued in the LS-PrePost software and the simulation itself was carried out in the LS-DYNA

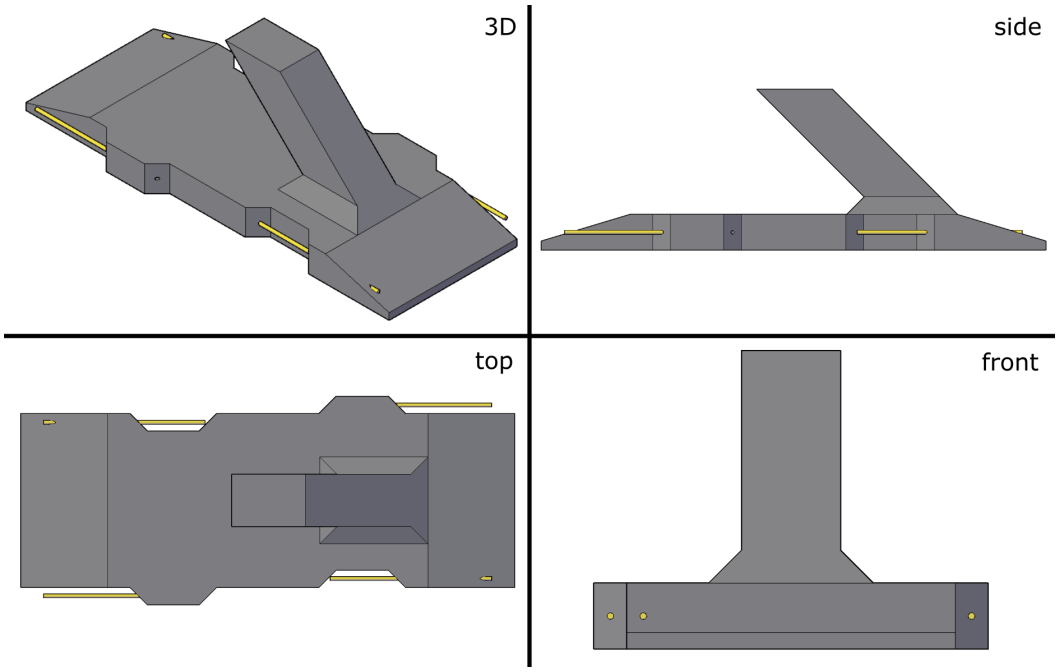

FIGURE 1. Model of the barrier. Connecting or locking steel bars are highlighted in yellow.

Parameter	Specification
Barrier dimensions	1 000 mm width, 2 850 mm length, 900 mm height
Concrete weight	1 300 kg
Total weight	1 460 kg
Concrete grade	C40/50
Welded steel brace	Base 2 × JA160/80/10, column 2 × U160, 40 mm rod diameter
Connecting steel rods	20 mm diameter
Steel brace and rods grade	S355
Reinforcing bars	16 mm diameter
Reinforcing bars grade	B500

TABLE 1. Summary of geometric and material characteristics of the barrier.

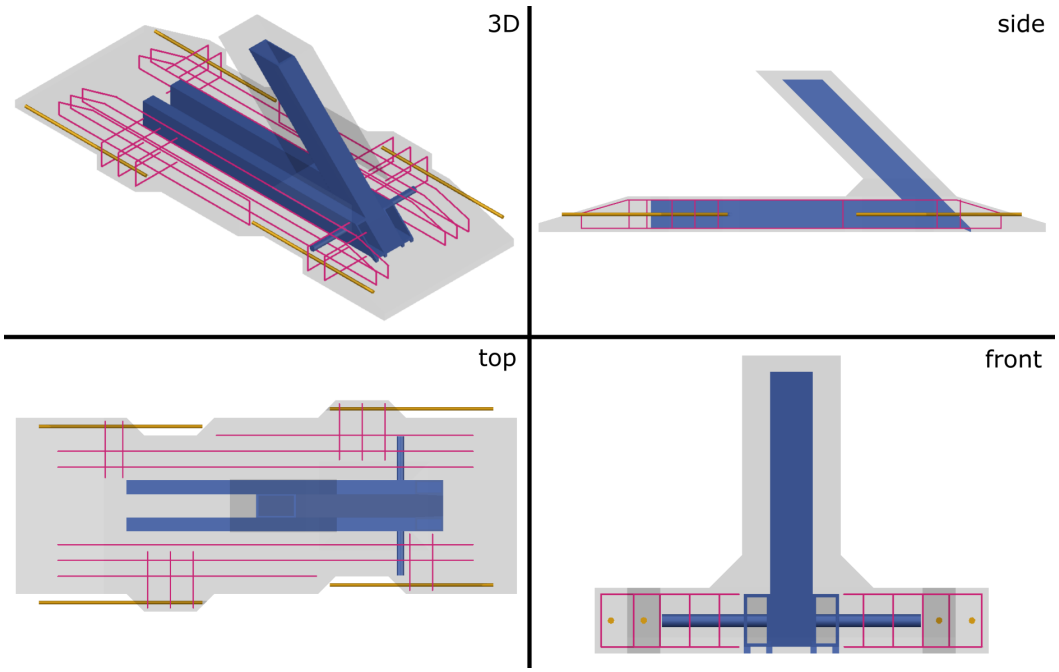

FIGURE 2. Steel elements inside the barrier. The main brace is highlighted in blue, the connecting or locking bars are in yellow and the concrete reinforcing bars are in red (drawn as axes without volume for clarity).

MID	RO	NPLOT	INCRE	IRATE	ERODE	RECOV	ITRETRC
1	2.5e-9	1	0	1	1.9	0	0
PRED							
0							
FPC	DAGG	UNITS					
50	8	2					

Table 2. Parameters of material model number 159 for LS-DYNA. Units: MPa, mm, s, $\mathrm{Mg\,mm^{-3}}$, N.

MID	RO	E	PR	SIGY	ETAN	FAIL	TDEL
2	7.85e-9	2.1e+05	0.3	355	3.55	0	0

Table 3. Parameters of material model number 24 for LS-DYNA. Value of SIGY was 355 for steel profiles and 500 for reinforcing bars. Units: MPa, mm, s, $\mathrm{Mg\,mm^{-3}}$, N.

Figure 3. Welded steel profiles forming the barrier's brace. In the back is the custom steel mould, note the upside-down orientation for casting concrete.

software. The simplified material models chosen for concrete and steel inside the barrier were materials number 159 (*MAT_CSCM_CONCRETE) and 24 (*MAT_PIECEWISE_LINEAR_PLASTICITY), respectively. The parameters of the models are given in Tables 2 and 3. The concrete was chosen to be of a generic precast structural type with an expected strength of 50 MPa and 8 mm maximum aggregate size, and the steel profiles the structural steel with a yield strength of 355 MPa and the concrete reinforcement bars with a yield strength of 500 MPa.

The load was simulated using a Ford F800 cargo truck model created by the National Crash Analysis Center. The model is available in the public domain. The parameters and geometry of the vehicle model were kept without changes, except for the weight of its load, which was changed so that the total weight of the vehicle was 7 500 kg. The speed at the moment of impact was set to $50\,\mathrm{km\,h^{-1}}$. The surface was simulated using a simple rigid plane, using *RIGIDWALL_PLANAR keyword. One plane was modelled to support only the vehicle without friction, and a second plane to support only the barriers with a friction coefficients of 0.4, 0.5, 0.6, and 0.7 in four separate versions of the simulation. This was done as the actual coefficient is unknown and will depend on the specific deployment location anyway, since the surface quality differs. However, this range of values is believed to be a reasonable estimate. As outlined in the Introduction, this is clearly a very simplified simulation approach. A more realistic interaction with a higher accuracy would be achieved by meshing the surface and using appropriate techniques to suitably achieve its high local deformations and cutting. However, such realistic behaviour would require a significantly computationally demanding simulation, which went beyond the scope of this research, considering the fact that only the basic estimate of the barrier's behaviour was needed, since it would be verified by the experiments. Five connected barriers were simulated, with the vehicle aiming at the centre one. The initial state is shown in Figure 4.

The total number of elements was 268 804, while one barrier that included all steel parts had 47 146 elements. The meshing was performed automatically in the Ansys Mechanical software. The barrier's concrete mass and steel brace were meshed using tetrahedron elements in order to better fit their geometry. Element formulation number 13, one point constant stress with nodal pressure averaging, was used. The locking bars were meshed using hexahedrons with element formulation number 1, constant stress solid element. Reinforcing bars inside the concrete were simulated using one-dimensional beam elements with beam element formulation number 1, Hughes-Liu with cross-section integration with tubular definition. This beam reinforcement is then embedded in the concrete using the keyword/function *CONSTRAINED_BEAM_IN_SOLID (which is a currently recommended replacement for keyword *CONSTRAINED_LAGRANGE_IN_SOLID for modelling concrete rebar). This technique does not require modelling of voids inside the concrete mass to fit the

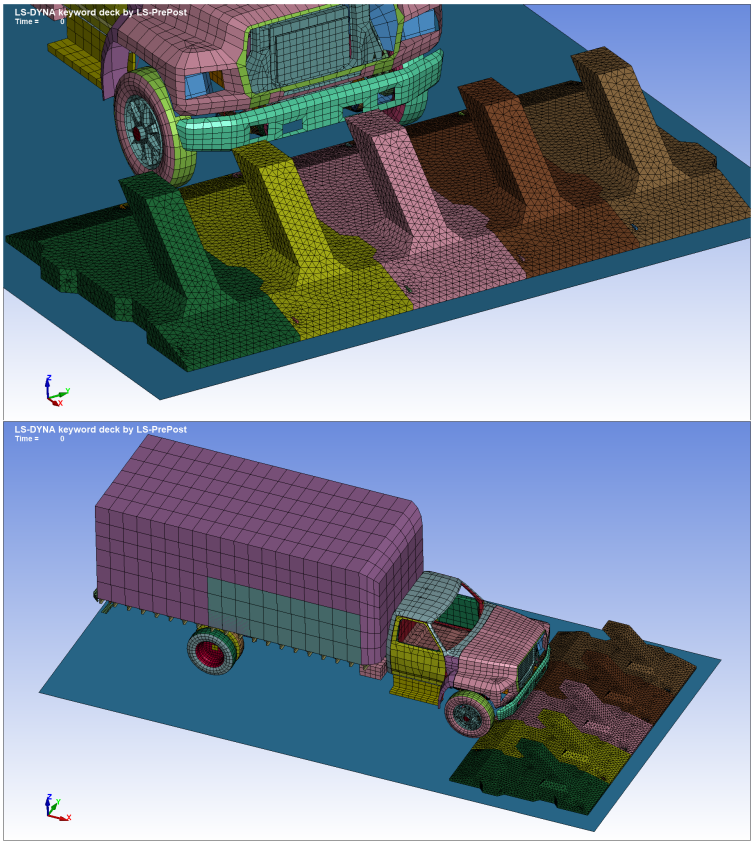

FIGURE 4. The initial state of the simulations.

reinforcing bars, but rather model the concrete as if it was unreinforced and add the beam reinforcement later. This approach is very computationally efficient with good accuracy [20].

After the crash test results were obtained, another set of simulations was conducted with improved parameters to better fit the crash test behaviour. The behaviour of the locking bar was of particular interest, so its model was changed. The parameters of the concrete and steel materials remained the same, as did the mesh of the steel brace and the reinforcement bars. The mesh of the locking bars was changed together with a slight improvement of the barrier mesh. Figure 5 shows this difference. The pre-crash simulations used a hexagonal cross-section of the locking bar, meshed with a relatively large number of hexahedra elements, accompanied by a perfectly matching mesh of the surrounding concrete with no tolerances. The post-crash version used a square cross-section, with a side length of 17.5 mm, in order to achieve the same second moment of inertia as a 20 mm diameter cylinder. This led to higher-quality elements of the locking bar as well as of the surrounding concrete (the pre-crash locking bar had 660 elements, while post-crash had 32). A tolerance of 0.5 mm was introduced around the bars, as well as between the concrete barriers. The rationale behind these changes was to prevent unrealistic seizing of the tightly pressed locking bar inside the barrier. The frictional coefficients of the surface plane were the same as for the pre-crash simulations,

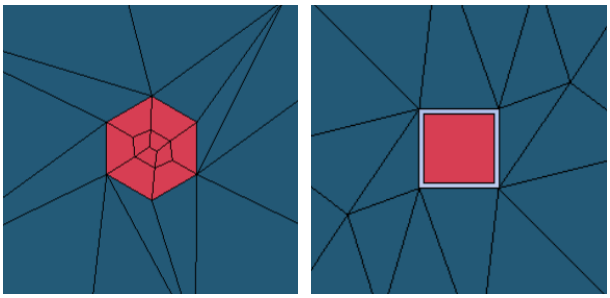

(A). Pre-crash simulations. (B). Post-crash simulations.

FIGURE 5. Versions of the locking bars.

extended with an additional 0.3 simulation. The optimised barrier used 38 640 elements, so the simulation had 226 274 elements in total.

2.3. CRASH TEST SETUP

Two full-scale crash tests were conducted using ordinary Renault Midlum and Fiat Ducato road vehicles. The parameters of the vehicles are summarised in Table 4 and the states right before the crash can be seen in Figure 6. Both vehicles were towed using an automatically detachable pulley system to reach an impact velocity of approximately 50 km h^{-1}. The impact was monitored by stationary cameras and an overhead drone. The vehicles were equipped with RIO and Racelogic PerformanceBox recording devices and radio-controlled pneumatic braking, which was

Vehicle	Length	Width	Height	Wheelbase	Total impact weight	Barrier setup
Renault Midlum, large goods vehicle	8 200 mm	2 500 mm	3 650 mm	4 450 mm	7 490 kg	5 barriers, impacting to the centre
Fiat Ducato, van	5 005 mm	1 998 mm	2 150 mm	3 200 mm	1 712 kg	3 barriers, impacting between centre and side barriers

Table 4. Summary of the two crash test setups.

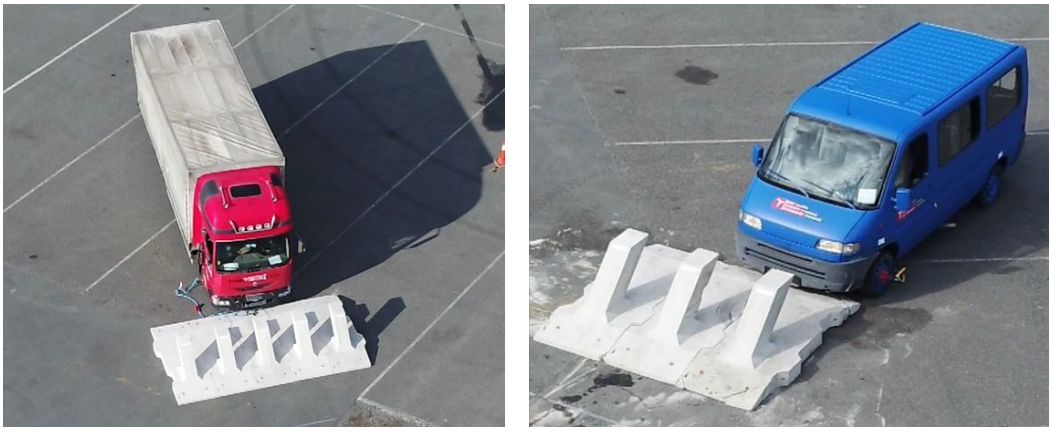

(a). Renault Midlum – 5 barriers. (b). Fiat Ducato – 3 barriers.

Figure 6. Crash test setups.

activated remotely after the crash for safety. Two tests were conducted due to the limited availability of vehicles, which led to the choice of different barrier setups compared to the numerical simulations, in order to assess a broader range of possible scenarios. The heavier vehicle was impacting five barriers, as it is expected that such a setup will be used realistically in places where such threat is possible. In smaller areas or narrower urban environments, the maneuverability of the attacking vehicle would be limited, therefore, it is likely that the threat would come from a smaller vehicle. Such a place would also fit fewer barriers, so three were chosen for the crash test with the van. The impact was also chosen to be aimed between the centre and one of the side barriers, to assess this loading scenario in a full-scale experiment.

3. Results and discussion

3.1. Numerical simulations

Figure 7 shows the progression of the crash simulation for the friction coefficient of the surface of 0.5. Other coefficient values showed small differences in the barrier behaviour, with the only major difference being the stopping distance. The left column of pictures shows the pre-crash simulations, and the right column shows the post-crash simulations. The plastic deformation, which for the concrete material represents the damage parameter of the CSCM model, is shown. The red colour represents elements of heavily cracked concrete, which then erode to simulate the breaking of the barrier. Figure 8 shows the complete model after the vehicle fully stopped, again, for both pre- and post-crash simulations. The simulation results cab be considered as a success, as the vehicles were stopped effectively. The concrete was extensively damaged, especially the central impacted barrier and its two neighbours. The centre barrier started to become incohesive due to this extensive damage, but despite that, the system performed well. The steel brace of the centre barrier was rotated from the concrete base and partially lodged in the vehicle's engine compartment. The brace itself saw minor plastic deformation. The major difference between the simulations was the locking bar behaviour. The pre-crash model showed all barriers remaining locked, whereas the post-crash model exhibited locking failure. This behaviour and the stopping distances of different friction coefficients are compared with the real crash test results in the following section.

3.2. Crash tests

The progression of the crash experiment with the large goods vehicle is summarised in Figure 9. It can be seen that immediately following the contact, the barrier lock failed between barriers two and three (counting from the left), leading to decreased mass available to react to the vehicle's kinetic energy. However, the impacted barrier performed as expected and the vehicle stopped at a distance of approximately 10.3 m with an average deceleration of 2.98 m s^{-2}. Figure 10 shows the situation after the crash. The concrete column of the centre barrier fell apart, as in the simulations,

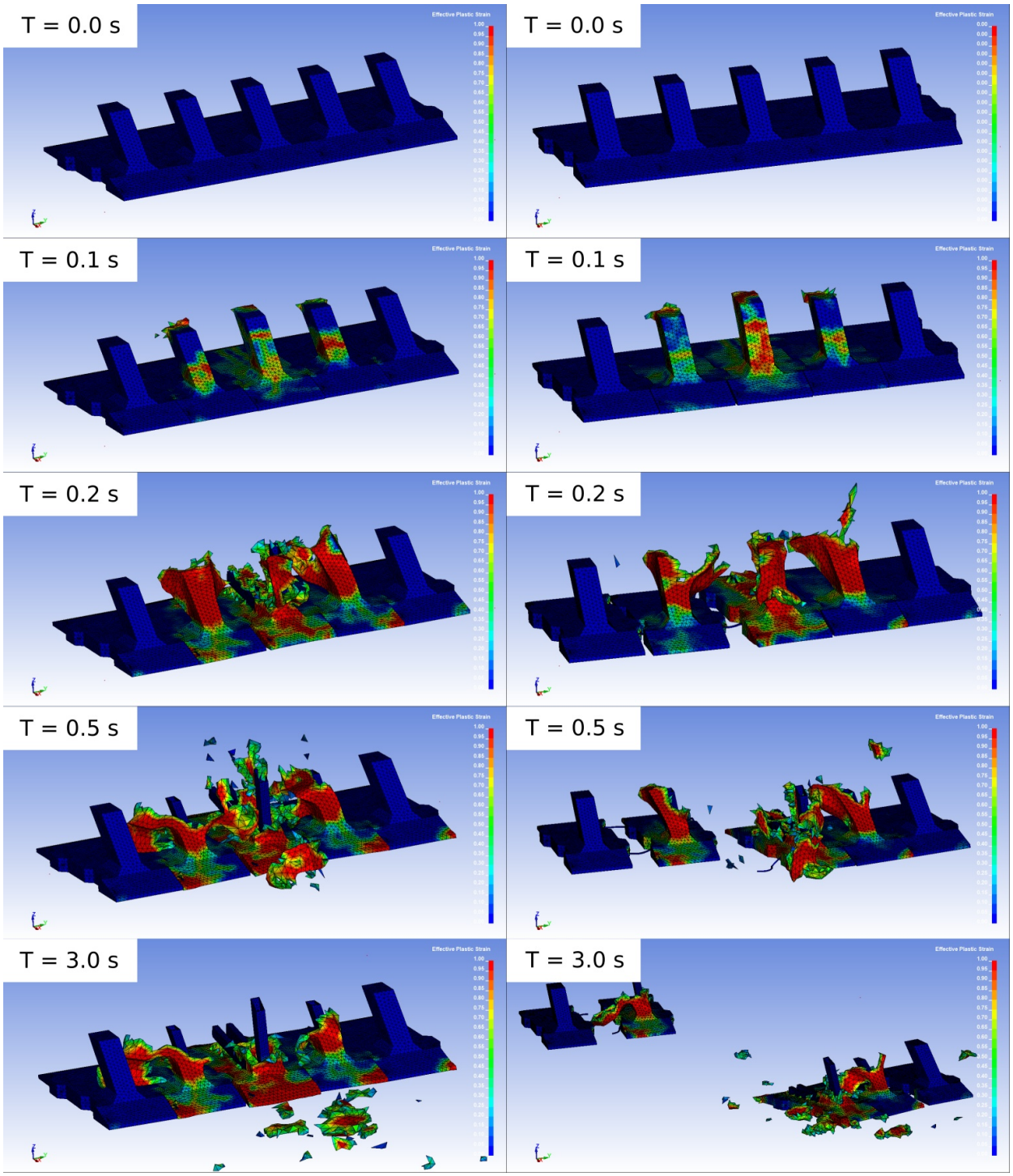

FIGURE 7. Progression of the numerical simulations. Crashing vehicle omitted for clarity. Left column – pre-crash simulations. Right column – post-crash simulations. Both for frictional coefficient of the plane of 0.5.

and the steel brace remained functional without showing any noticeable plastic deformation. The rest of the concrete volume was heavily damaged and largely incohesive, which is also in-line with the simulations. The locking system of the centre barrier eventually fell apart, but from the crash progression videos it is clear that the steel locking bars were the first to fail. Figure 10 also highlights the failed locking bar, which resulted in barriers 1 and 2 staying practically out of the crash, remaining undamaged. This behaviour was not observed for the pre-crash simulations and is considered significantly negative for the entire system's performance. This knowledge led to changes for the post-crash simulations, as described in Section 2.2. This new simulation validated this behaviour accurately. As seen in the comparison in Figure 10, the locking bars failed identically. When comparing Figures 9 and the right columns of Figures 7 or 8, even the asymmetry of the resulting situation was well captured, with barriers 1 and 2 pushed aside. However,

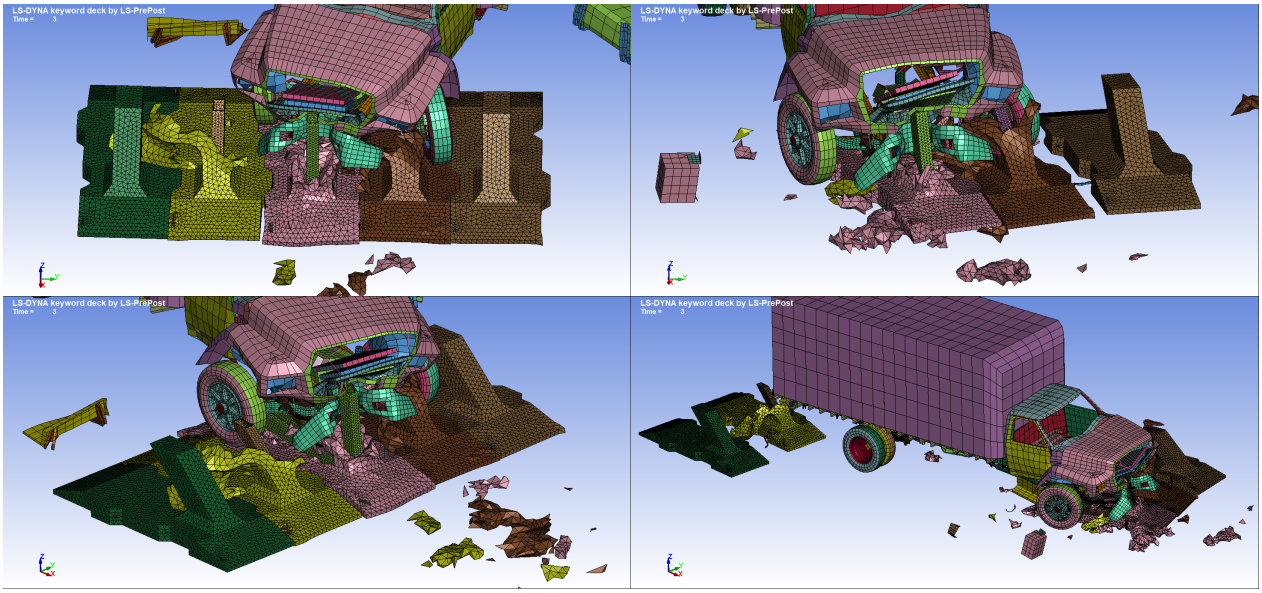

Figure 8. State of the barriers and the impacting vehicle after it fully stopped. Left column – pre-crash simulations. Right column – post-crash simulations. Both for frictional coefficient of the plane of 0.5.

Figure 9. Progression of the crash test with the large goods vehicle.

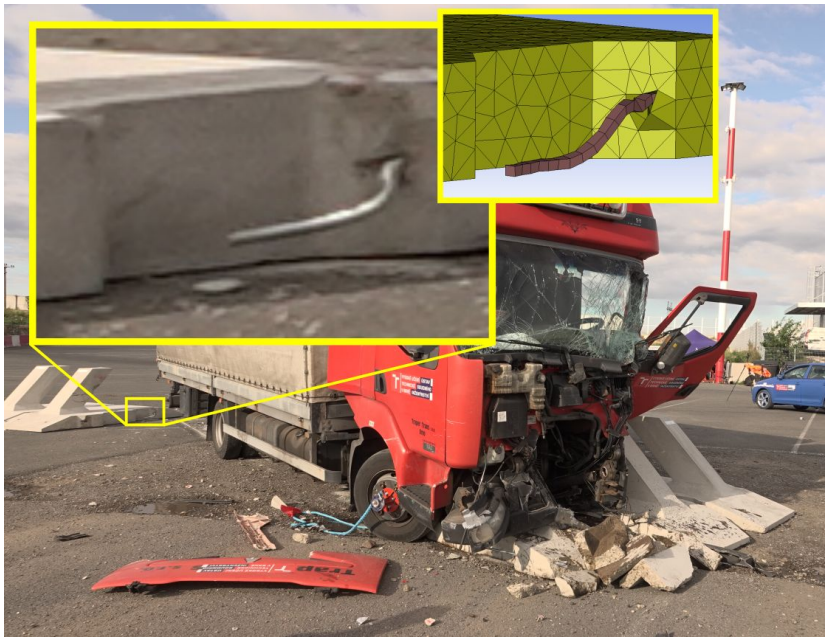

Figure 10. State after the vehicle stopped, first crash test. Highlight shows the failed interlocking bar, which slipped from the neighbouring barrier due to its excessive deformation.

FIGURE 11. Progression of the crash test with the van.

in the post-crash simulations, the column of barrier 2 was destroyed, unlike in the experiment. Nevertheless, the post-crash simulations confirmed the problem of too tightly pressed locking bars in the concrete volume and captured the experiment's behaviour well.

The progression of the second crash test is summarised in Figure 11. The overall behaviour is similar to that of the first test, proportional to the lower weight of the van. The van has stopped at a distance of 3.9 m with an average deceleration of 4.87 $\mathrm{m\,s^{-2}}$. Figure 12 shows the final state. Once again, the interlocking bars proved to be the weakest point. The centre barrier's column was heavily damaged, but less so compared to the first crash. The remainder of the barrier's volume remained largely cohesive. Notable is also the behaviour of the concrete debris. In case of a crash in an urban environment, this could be dangerous, as it is known that secondary fragments formed after an extreme loading event can cause further damage [21, 22]. Nevertheless, it can clearly be seen that only very small fragments fell further from the crash site, while large concrete pieces remained close to the barrier. To minimise or practically eliminate such debris, fibre-reinforced concrete with an appropriately designed concrete matrix should be used. However, that would increase the cost of the barrier and exposed steel fibres would be dangerous to passers-by, necessitating further surface treatment.

4. Stopping performance

The most important result of the simulations and crash tests are the stopping distances. These are summarised in Table 5. The stopping distances were measured as the difference between the initial front of the barrier (away from the vehicle) and the furthest point of the vehicle penetration, in the axis of the crash. The large goods vehicle experiment would be classified as PAS 68:2013 Road blocker V/7 500(N2)/48/90:10.3/0 and the van experiment as PAS 68:2013 Road blocker V/1 500(N1)/56/90:3.9/0. Overall, the pre-crash simulations exhibited lower stopping distances, because they did not experience the locking bar failure, and therefore resulting in greater reaction weight against the vehicle. The post-crash simulations all experienced the locking bar failures and the stopping distances are significantly higher. The pre-crash simulations then presented a sort of showcase of what the barriers should be capable of if the locking mechanism was improved – in this case, an improvement in stopping distances of roughly 2 m. The post-crash simulation for the frictional coefficient of 0.4 still resulted in a lower stopping distance compared to the experiment, which is the reason why the additional 0.3 case was simulated as well. However, the stopping distance was excessively long, at 15.2 m, with the barriers sliding unrealistically. The rigidwall plane surface approach in this case (asphalt-concrete sliding in a crash test) could be used, but the friction coefficient should not be higher than 0.4 or 0.3 for safety margins.

FIGURE 12. State after the vehicle stopped, second crash test. Note the bent interlocking bar in the front-left of the barrier.

Case	Stopping distance
Large goods vehicle	10.3 m
Van	3.9 m
Simulation pre 0.4	7.5 m
Simulation pre 0.5	5.7 m
Simulation pre 0.6	4.5 m
Simulation pre 0.7	3.8 m
Simulation post 0.3	15.2 m
Simulation post 0.4	9.6 m
Simulation post 0.5	9.3 m
Simulation post 0.6	8.6 m
Simulation post 0.7	5.7 m

TABLE 5. Summary of stopping distances.

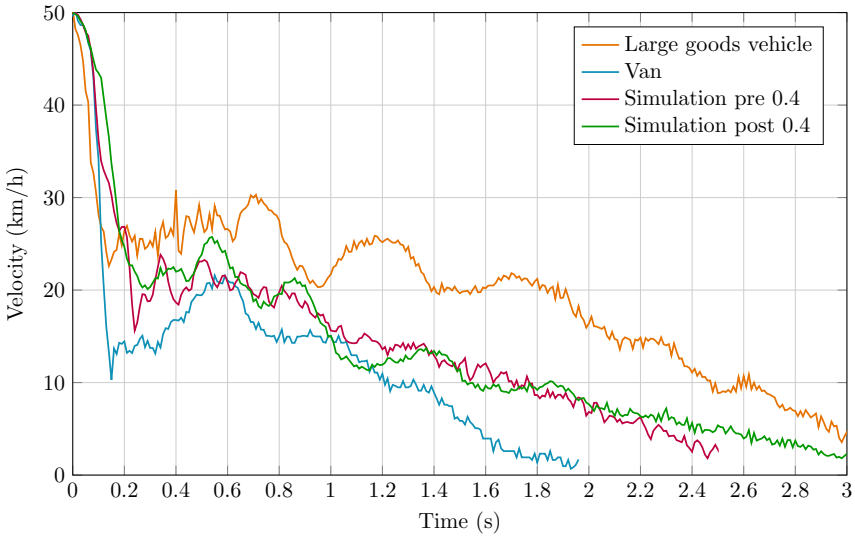

Figure 13. Comparison of the measured deceleration data and the numerical simulations.

The graph in Figure 13 shows a comparison of the measured velocity from the crash test and as obtained from the simulations. An element from the back of the driver's cabin was chosen to plot the simulation data, as that area did not see any damage. Only the 0.4 frictional coefficient cases are plotted for clarity. The crash can be divided into three phases. The first is the initial contact, during which the kinetic energy of the vehicles is dissipated rapidly by overcoming the inertia of the stationary barriers and cracking the concrete volume. This phase is very similar between the two crash tests and in good agreement with the simulations. The simulations are practically identical in this phase, as the surface friction plays a negligible role in this interaction. The large goods vehicle slows down less, most likely due to those two disconnected barriers. The van slows down more because it is significantly lighter, despite the fewer barriers used. The second phase is a short rebound of the vehicles, when they seemingly gain velocity. This is due to the tracking of one point in the deforming vehicle that exhibited an oscillation. Similarly, this can be observed for the simulation data, but because an inner, likely more rigid point, of the vehicle was tracked, this oscillation is minimal. The third phase is when the vehicle's parts stabilise and the friction of the barrier-surface contact slows down the vehicle until a full stop. This is the phase that differs the most.

This graph shows the two primary interaction principles with which the barrier needs to work and their influence. In this case, the initial velocity loss was roughly 50 %. It seems logical that this phase should be improved as much as possible. This phase was caused by the weight of the barrier, so increasing its weight is beneficial for improving stopping performance. An obvious solution, however, it goes against the idea of a mobile, quick-to-deploy barrier. Although there are heavy trucks equipped with hydraulic arms capable of lifting much heavier loads, the smaller hydraulic arms are limited to roughly 1.5 tonnes, which is the current weight of one barrier. The barriers will also be placed in a rather long line requiring a long arm reach, decreasing the lifting capacity. Several barriers will also be needed, so the total transport capacity is also a key variable. All of this must be considered if a rapid deployment is of concern. However, too light barrier is not optimal as it can be, for example, simply moved aside prior to an attack or stolen if not guarded.

The second principle concerns the vehicle-barrier and barrier-surface interactions, which are responsible for the final stopping of the vehicle, so in this case, for slowing the vehicle down by approximately the remaining half of its initial velocity. The vehicle-barrier interaction is created by the vehicle pushing down on the base of the barrier with its front wheels. This means that the barrier can almost immediately, after the initial contact, start slowing the vehicle down due to the barrier-surface friction. This friction is a crucial part of the performance of a mobile barrier. In this case, a flat bottom surface of the barrier was chosen as it is the simplest manufacturing option. However, providing the bottom with an additional rough metal structure would likely improve this interaction. The relatively large difference in velocities between the large goods vehicle and both simulations in Figure 13 from roughly 0.6 s forward is likely due to the weakness of the simplified rigid surface approach, which is unable to capture the damage (and subsequent changes in surface-object interactions) that clearly occurred to the asphalt surface in the experiment.

5. Conclusion

In this study, a protective mobile urban barrier was designed, numerically simulated, and tested in real crash-test scenarios. Overall, the barrier system performed adequately, but shortcomings were identified, especially related to the interlocking mechanism, which in

our case failed during the real crash test experiments. Several key observations were made, and they can be summarised as follows.

- The geometry of the designed barrier, combined with the steel reinforcement, is effective.
- The weight of a single barrier of 1.5 tons is adequate considering the combined needs for transportation, deployment, and stopping performance.
- This type of barrier and stopping principle can be numerically simulated with simplified surfaces with reasonable accuracy, if such a basic evaluation is desired. However, the coefficient of friction should be set to a rather low value, below 0.4, to account for this simplification and safety margins.
- The interlocking mechanism responsible for keeping the barrier system connected throughout the crash must be designed (and numerically simulated) with great care, as its failure significantly affects the performance.
- Since the weight principle cannot be increased further due to the aforementioned requirements, these barriers need specifically improved vehicle-barrier and barrier-surface interactions. The stopping power of the system's weight also comes from a well-functioning interconnection mechanism, further stressing its importance.
- A concrete barrier would benefit from using dispersed fibre reinforcement and a high-performance matrix, as it would limit the formation of debris.

Acknowledgements

The authors gratefully acknowledge the financial support from Operational Programme Enterprise and Innovation for Competitiveness, grant number CZ.01.1.02/0.0/0.0/20_321/0025143.

References

[1] D. Markovic, A. Scattina, M. Larcher. Impact load characterization for security barrier performance assessment through simulations using generic vehicle models. *International Journal of Protective Structures* **16**(1):266–290, 2024. https://doi.org/10.1177/20414196241286158

[2] G. R. Consolazio, J. H. Chung, K. R. Gurley. Impact simulation and full scale crash testing of a low profile concrete work zone barrier. *Computers & Structures* **81**(13):1359–1374, 2003. https://doi.org/10.1016/S0045-7949(03)00058-0

[3] A. Grana, N. Dinnella, S. Chiappone. Enhancing road safety with the infrastructure-adaptable NDBA 2.0 concrete median barrier: An Italian experience. *Archives of Transport* **71**(3):147–168, 2024. https://doi.org/10.61089/aot2024.1bp10d20

[4] S. Baragetti, E. V. Arcieri. Study on a new mobile anti-terror barrier. *Procedia Structural Integrity* **24**:91–100, 2019. https://doi.org/10.1016/j.prostr.2020.02.008

[5] B. Hu. An assessment of current maximum impact force models for anti-ram bollard systems subjected to truck impact. *International Journal of Protective Structures* **8**(3):368–383, 2017. https://doi.org/10.1177/2041419617721551

[6] Y. Zhou, L. Reese, T. Qiu, Z. Rado. Field test and numerical modeling of vehicle impact on a boulder with impact-induced fractures. *International Journal of Protective Structures* **7**(1):3–17, 2016. https://doi.org/10.1177/2041419615622725

[7] L. Reese, T. Qiu, D. Linzell, et al. Field tests and numerical modeling of vehicle impacts on a boulder embedded in compacted fill. *International Journal of Protective Structures* **5**(4):435–451, 2014. https://doi.org/10.1260/2041-4196.5.4.435

[8] N. Buckley. The design and testing of a portable vehicle crash barrier. In *38th Annual 2004 International Carnahan Conference on Security Technology*, pp. 47–55. 2004. https://doi.org/10.1109/CCST.2004.1405368

[9] M. Dubánek, J. Lakosil, P. Minařík. *Utajená obrana železné opony: československé opevnění 1945–1964 [In Czech; Secret defense of the Iron Curtain: Czechoslovak fortifications 1945–1964]*. Mladá fronta, 2008. ISBN 978-80-204-1758-9.

[10] M. Mára, P. Konrád, J. Fornůsek, et al. Development of mobile road barrier made of ultra-high-performance fibre-reinforced concrete. *Materials Today: Proceedings* **32**:162–167, 2020. https://doi.org/10.1016/j.matpr.2020.04.182

[11] P. Konrád, M. Mára, J. Fornůsek, et al. Mobile anti-vehicle barrier made of high-performance fibre-reinforced concrete. *Advances in Structural Engineering* **24**(11):2364–2374, 2021. https://doi.org/10.1177/1369433221997728

[12] P. Konrád, R. Sovják. Experimental procedure for determination of the energy dissipation capacity of ultra-high-performance fibre-reinforced concrete under localized impact loading. *International Journal of Protective Structures* **10**(2):251–265, 2019. https://doi.org/10.1177/2041419618819506

[13] S. Kravanja, R. Sovják, P. Konrád, J. Zatloukal. Penetration resistance of semi-infinite UHPFRC targets with various fiber volume fractions against projectile impact. *Procedia Engineering* **193**:112–119, 2017. https://doi.org/10.1016/j.proeng.2017.06.193

[14] R. Lovichová, M. Mára, J. Fornůsek. Projectile impact resistance of UHPFRC structures for various methods of fresh mixture placement. *Procedia Engineering* **193**:80–87, 2017. https://doi.org/10.1016/j.proeng.2017.06.189

[15] National Protective Security Authority. Public realm design guide for hostile vehicle mitigation, 2023. [2025-06-01]. https://www.npsa.gov.uk/public-realm-design-guide-hostile-vehicle-mitigation-0

[16] D. Aggromito, J. Farley, M. Walden. Application of vehicle impact simulation for protective barrier design. In *12th European LS-DYNA Conference 2019*, pp. 1–10. 2019.

[17] M. Andrae, D. Markovic, R. Schumacher, et al. Methodology for numerical simulations of vehicle impact on security barriers considering soil-barrier interaction. *Publications Office of the European Union* (KJ-NA-31-844-EN-N), 2024. https://doi.org/10.2760/33565

[18] T. K. Yoo, T. Qiu, L. Reese, Z. Rado. Field testing and numerical investigation of streetscape vehicular anti-ram barriers under vehicular impact using FEM-only and coupled FEM-SPH simulations. *International Journal of Protective Structures* **7**(2):213–231, 2016. https://doi.org/10.1177/2041419616652527

[19] M. Y. Apak, M. Ergun, H. Ozen, et al. Finite element simulation and failure analysis of fixed bollard system according to the PAS 68:2013 standard. *Engineering Failure Analysis* **135**:106151, 2022. https://doi.org/10.1016/j.engfailanal.2022.106151

[20] L. Moutoussamy, G. Hervé-Secourgeon, F. Barbier. Qualification of *CONSTRAINED_LAGRANGE_IN-_SOLID command for steel/concrete interface modeling. In *8th LS-Dyna European User Conference*, pp. 1–11. 2011. https://doi.org/10.13140/2.1.4530.4326

[21] Ø. E. K. Jacobsen, M. Kristoffersen, S. Dey, T. Børvik. Sustainable shielding: Ballistic performance of low-carbon concrete. *Construction and Building Materials* **415**:135103, 2024. https://doi.org/10.1016/j.conbuildmat.2024.135103

[22] A. Kumar, M. Iqbal. Experimental investigation of ballistic evaluation of reinforced concrete slabs with and without shear reinforcement against hard projectile impact. *Engineering Structures* **328**:119793, 2025. https://doi.org/10.1016/j.engstruct.2025.119793